frontiers in Materials

ORIGINAL RESEARCH
published: 25 September 2019
doi: 10.3389/fmats.2019.00235

Cellulose Nanowhisker (CNW)/Graphene Nanoplatelet (GN) Composite Films With Simultaneously Enhanced Thermal, Electrical and Mechanical Properties

Dongyan Liu[1], *Yu Dong*[2], *Yueyue Liu*[1], *Na Ma*[1] *and Guoxin Sui*[1]*

[1] *Institute of Metal Research (IMR), Chinese Academy of Sciences, Shenyang, China,* [2] *School of Civil and Mechanical Engineering, Curtin University, Perth, WA, Australia*

Transparent cellulose nanowhisker (CNW)/graphene nanoplatelet (GN) composite films were produced via sonication mixing and solution casting methods. Such composite films exhibited improved thermal, electrical and mechanical properties. The material morphologies and microstructures were examined using scanning electronic microscopy (SEM), X-ray diffraction (XRD) analysis and Raman spectroscopy. Strong interaction was detected when CNWs were randomly attached onto graphene sheets, as evidenced by SEM images obtained in this study. In particular, the addition of GNs into CNWs had significant effect on the thermal behavior of composite films. The melting temperature (T_m) and initial thermal decomposition temperature (T_{id}) of CNW films were both increased by 23.2, 29.3, 26.3°C, and 70.2, 88.4, 87.8°C with the inclusions of 0.1, 0.25, and 0.5 wt% GNs, respectively. The electrical conductivity of composite films was enhanced in a monotonically increasing manner with the maximum level of 4.0×10^{-5} S/m detected at the GN content of 0.5 wt%. Their tensile strength was also improved by maximum 33.7% when increasing the GN content up to 0.25 wt% as opposed to that of CNW films. Such CNW/GN composite films can be potentially used in green anti-static and electronic packaging applications.

Keywords: cellulose nanowhiskers (CNWs), graphene nanoplatelets (GNs), electrical conductivity, thermal stability, mechanical strength

OPEN ACCESS

Edited by:
Luca Valentini,
University of Perugia, Italy

Reviewed by:
Veronique Michaud,
École Polytechnique Fédérale de Lausanne, Switzerland
Claudia Merlini,
Federal University of Santa Catarina, Brazil

***Correspondence:**
Guoxin Sui
gxsui@imr.ac.cn

Specialty section:
This article was submitted to Polymeric and Composite Materials, a section of the journal Frontiers in Materials

Received: *22 July 2019*
Accepted: *09 September 2019*
Published: *25 September 2019*

Citation:
Liu D, Dong Y, Liu Y, Ma N and Sui G (2019) Cellulose Nanowhisker (CNW)/Graphene Nanoplatelet (GN) Composite Films With Simultaneously Enhanced Thermal, Electrical and Mechanical Properties. Front. Mater. 6:235. doi: 10.3389/fmats.2019.00235

INTRODUCTION

Cellulose is one of the most widely used polymers in nature with the annual production of approximately 5×10^{11} tons on earth (Yuan et al., 2015). Cellulose nanowhiskers (CNWs) are generally extracted from natural cellulose-based materials including plants, bacteria, and sea creatures by using hydrolysis methods. It is sized by several nanometers to a few tens of nanometers in diameter and several 100 nm in length. CNWs possess high elastic modulus, large aspect ratios and surface areas, and are generally deemed as ideal reinforcing fillers in polymer composites. Being a natural nanosized polymer, CNWs can be manufactured into different multifunctional composite materials. In view of the wide applications of CNWs, it has been demonstrated that CNWs are

considered as one of the most important material components in waste water treatment (Carpenter et al., 2015; Karim et al., 2016), drug delivery (Jackson et al., 2011), electronic devices (Li and Lee, 2017), energy storage (Xing et al., 2019), food packaging (Li F. et al., 2015), etc. Jiang et al. (2015) reported that the UV-blocking ratios of nanocellulose/6wt% ZnO transparent composite films reached 97.8% and 99.1% at the wavelengths of 300 and 225 nm, respectively. Zhan et al. (2018) successfully prepared UV-induced and self-cleanable nanocellulose/TiO_2 composite membranes in possession of effective separation for various surfactant-stabilized emulsions with high oil rejection over 99.5%. Sadasivuni et al. (2016) demonstrated ultra-flexibility and high-level NO_2 sensitivity of iron oxide @ cellulose nanocrystal (CNC) composites. On the other hand, Meulendijks et al. (2017) and Drogat et al. (2011) proved that CNW/Ag composites had good electrical conductivity and antibacterial feature. As far as green materials and environmental sustainability are concerned, CNWs are gradually gaining more popularity in the development of functional nanomaterials.

Cellulose films are well known as a potential substrate/matrix for conductive materials due to its renewability, biodegradability and flexibility (Du et al., 2017; Agate et al., 2018). Because CNWs have excellent film formability and affinity with conductive polymers, they are widely used as CNW-based conductive ink (Latonen et al., 2017), sensors (Mahadeva et al., 2011; Esmaeili et al., 2015) and capacitors (Liew et al., 2013; Jose et al., 2019) when incorporated into conductive polymers (He et al., 2019). Carbon-based nanomaterials are functional nanofillers such as carbon nanotubes (CNTs) and graphene, which can be used for cellulosic materials when considering their extraordinary material properties including but not limited to electrical conductivity, mechanical strength and modulus, electromagnetic-shielding effectiveness and capacity. Yamakawa et al. (2017) reported a high electrical conductivity of 1.05 S/m, good mechanical properties such as high Young's modulus of 10.1 GPa and tensile strength of 173.4 MPa, as well as a low coefficient of thermal expansion (CTE) at 7 ppm/K. Pang et al. (2015) fabricated multifunctional cellulose/CNT composite papers using a filtration method. At the CNT contents of 10–71 wt% in the frequency range of 175–1,600 MHz, it was detected that such papers yielded an electrical conductivity of 9.9–216.3 S/m along with good electromagnetic interference (EMI) shielding effectiveness (SE) at 15–45 dB. In addition, these composite papers with the inclusion of 50 wt% CNTs possessed the capacitance of 46 F/g at a scan rate of 5 mV/s, reversible discharge capacity of 474.0 mAh/g when they were taken as an anode current collector for lithium ion battery (Pang et al., 2015). Dichiara et al. (2017) indicated that the addition of hydroxyl-functionalized CNTs with pre-absorbed alkali lignin gave rise to the improvement of dry and wet strengths of cellulose fibers along with good sensitivity of humidity. On the other hand, Ko et al. (2019) utilized a solution casting method to fabricate methyl cellulose/50 wt% CNT composite papers with a much higher electrical conductivity of 15.9 S/cm and better bending durability as opposed to those of graphene and indium tin oxide (ITO). Gnanaseelan et al. (2018) suggested cellulose/single-walled CNT (SWCNT) composite films should be considered as a promising thermoelectric material owing to their relatively high power factors when compared with those of other insulating polymer/CNT composites. In comparison with fiber-like CNTs, 2D graphene sheets could be a better nanofiller alternative, as evidenced by greatly improved tensile strength by 93% and significantly enhanced electrical conductivity by 10 folds in bacterial cellulose/graphene composite papers (Luo et al., 2019). More recently, Zhan et al. (2019) produced highly conductive cellulose nanofibrils/20 wt% exfoliated graphene composite films with a remarkable electrical conductivity of 568 S/m along with excellent mechanical properties including tensile strength of 389 MPa, elastic modulus of 8.0 GPa and elongation at break of approximately 20%. The associated multifunctional properties of cellulose composites are summarized in **Table 1** accordingly.

Nanocellulose/graphene composites are deemed as ideal electrode materials for flexible supercapacitors (Xing et al., 2019). The potential use of cellulose-based nanomaterials sheds light on widespread applications in material conductivity, energy storage and electronic devices, etc. The excellent material properties of cellulose and CNTs or graphene rely on their linkages by non-covalent interactions with well-maintained intrinsic properties of both nanomaterials. CNWs have been proven to be an effective aqueous-based dispersant for 2D nanosheet materials due to their unique characteristics of nanoscale size, surface charge and molecular chain structures (Li F. et al., 2015; Ma et al., 2017). Polyurethane sponges with superhydrophobicity and superamphiphilicity were produced by a simple dip-coating method, which was derived from the close interaction between CNWs and graphene (Zhang et al., 2017, 2018). Such an interaction can be confirmed not only from material morphologies, structural changes, but also from the characteristic peaks on thermal analysis. The thermal behavior can indicate the interaction between polymeric molecular chains and reinforcing fillers. In general, glass transition temperature (T_g), melting temperature (T_m), initial decomposition temperature (T_{id}) can be altered significantly with their strong interaction.

Nanocellulose/GN composites have been extensively studied for their mechanical and electrical properties. Nonetheless, thermal properties of CNW films and their composites may not be well investigated. Our initial work (Ma et al., 2017; Zhang et al., 2017, 2018) focused on the interaction between CNWs and GNs, and found that a small addition of GNs could greatly increase melting temperature and decomposition temperature of CNW films, which was ascribed to morphological absorption and enhanced physical parameters upon heating. The research objective and novelty of this study lie in the successful development and holistic evaluation of CNW/GN composite films in relation to the GN role as rigid fillers as well as filler-matrix interactions to simultaneously enhance their thermal, electrical and mechanical properties, which may be hard to achieve in conventional nanocomposite materials so that CNW/GN composite films are expected to be potentially effective multifunctional materials for electronic packaging applications.

EXPERIMENTAL WORK

Materials

Industrial flax linens as raw materials were purchased from Xuyi Textile Material Co. Ltd (Ningbo, China) for CNW extraction.

TABLE 1 | Multifunctional properties of cellulose composites.

Filler/Content	Method	Properties	References
6 wt% ZnO	Pressure extrusion Vacuum-oven drying	UV blocking ratios of 97.79% and 99.13% for wavelengths of 300 and 225 nm	Jiang et al., 2015
TiO_2	Filtration Vacuum-oven drying	Self-cleanable, high oil rejection over 99.5%	Zhan et al., 2018
Fe_2O_3	*In situ* synthesis	NO_2 sensitivity: ppm level	Sadasivuni et al., 2016
Ag	*In situ* synthesis	Minimum inhibitory concentration: *E. coli* strain:2.7 μg/mL; *S. Aureus* strain: 5.4 μg/mL	Drogat et al., 2011
5 wt% multi-walled CNTs (MWCNTs)	Filtration	Electrical conductivity: 1.05 S/cm Young's modulus: 10.1 GPa Tensile strength: 173.4 MPa CTE: 7 ppm/K	Yamakawa et al., 2017
10–71 wt% CNTs	Filtration	Electrical conductivity: 9.9–216.3 S/m EMI SE: 15–45 dB Capacitance: 46 F/g @ 50 wt% CNTs	Pang et al., 2015
20 wt% GNs	Oven drying	Electrical conductivity: 568 S/cm	Zhan et al., 2019

Graphene nanoplatelets (GNs) were supplied in powder form by Sichuan Jinlu Group Co., Ltd, Deyang, China. GNs consist of 5–8 layers based on single graphene sheet. Their lateral size is around 10–20 μm, and the atomic ratio between C and O elements is 80–100. All other used chemicals including uranyl acetate, sodium hydroxide, concentrated sulfuric acid, glacial acetic acid, toluene, ethanol and hydrogen peroxide were obtained from Shenyang Dongbao Company (Shenyang, China) without modification.

Preparation of CNWs

CNWs were isolated from bleached flax yarns by using a sulfuric acid method, as previously reported (Liu et al., 2010). The yarns were heated in 60 wt% sulfuric acid for 1 h at 55°C, which was followed by consecutive dilution and washing processes repeatedly in a centrifuge tube until the supernatant is neutral. The aqueous suspension of CNWs was stored in a fridge for the further experimental use.

Preparation of CNW/GN Composite Films

GNs were added in suspension of 0.5 wt% CNWs at the GN contents of 0.1, 0.25, and 0.5 wt%. The homogeneous aqueous dispersion of GN/CNW mixture was obtained by ultrasonicating (KH-1600TDE, Kunshan, China) graphene powders and CNWs in deionized water at a frequency of 80 kHz and an electrical power of 1,600 W until the uniform dispersion was obtained. The GN aggregates were broken up into GN sheets and became stabilized in CNW suspensions. CNW/GN composite films were successfully prepared by casting the mixture onto a plastic petri dish, which was followed by water evaporation at ambient temperature. Final composite films were peeled off from the petri dish after being dried under the ambient condition, which were denoted as "CNWs/0.1 GNs," "CNWs/0.25GNs," and "CNWs/0.5GNs" at the GN contents of 0.1, 0.25, and 0.5 wt%, respectively in the following result section.

Characterization Methods

The morphology of CNWs was characterized using a transmission electron microscope (TEM, Philips CM 12, Holland) with an acceleration voltage of 100 kV. The aqueous CNW suspension was diluted to be 0.1g/L. A droplet of such suspension was dropped onto a copper grid covered with a carbon film. The samples were then stained with 2.0 wt% solution of uranyl acetate for 1 min prior to TEM observation.

The morphologies of CNW/GN composite films were observed on a field emission scanning electron microscope (JSM-6301F) at the accelerating voltage of 10 kV. The samples were sputter coated with gold about 10–20 nm in thickness prior to SEM observation. On the other hand, the photographs of CNW/GN composite films were recorded with a digital camera.

The electrical conductivity was measured by using a Keithley electrometer model 2000 (USA). Two round copper disks were used as the electrodes and their surfaces were polished and spread with silver paste in order to warrant good contact with the testing films. Volume resistance (R) was measured and the resistivity ρ was calculated as follows:

$$\rho = RS/t \quad (1)$$

$$\sigma = 1/\rho \quad (2)$$

where t is the film thickness in cm, S is the circular area of the film in cm^2, and subsequently corresponding electrical conductivity σ in S/m was calculated according to Equation (2).

Thermal behavior of films was studied using thermogravimetric analysis (TGA Q500, TA instruments, USA) and TA differential scanning calorimetry (DSC Q20, TA instruments, USA). Each sample weighing approximately 5 mg was heated from 50 to 800°C at a heating rate of 20°C/min for TGA while heated from 50 to 400°C at a heating rate of 10°C/min for DSC. Both thermal analyses were conducted under nitrogen atmosphere to prevent any thermoxidative degradation.

Wide-angle X-ray diffraction measurements were performed using a Rigaku D/max 2500PC diffractometer equipped with Cu Kα radiation (wave length $\lambda = 1.54$ Å) at 50 kV and 300 mA in the 2θ range of 5–50° with a step interval of 0.02° to study the influence of GNs on the crystalline structures of CNWs.

Raman spectroscopic measurement (JY Labram HR 800 spectrometer) was carried out to characterize the characteristic peaks of GNs at the wavelength of 632.8 nm under a laser power of 2.5 mW with 6 accumulations.

RESULTS AND DISCUSSION

Morphological Structures

Morphology of CNWs

CNWs used in this study were hydrolyzed with sulfuric acid. **Figure 1** demonstrates the TEM image of CNWs along with their aqueous suspensions at the CNW concentrations of 0.2 g/L (left) and 2 g/L (right). It is clearly seen that CNWs can be categorized as a nanosized polymer in rod shape with their diameter and length of approximately 30 and 500 nm, respectively. At the low CNW concentration about 0.2 g/L, their aqueous suspensions appear to be transparent similar to water. Whereas, with increasing the CNW concentration, milky colored suspensions gradually become evident. CNW dispersion in water is very stable because of their hydrophilicity and negatively charged surfaces with sulfate groups. As such, CNWs can be potentially used as the dispersant for other nanomaterials. The surface charges can be evaluated by Zeta potential, which means that the higher the potential, the more stable the dispersion is. It is one of the most vital factors for dispersing graphene aggregates (Ma et al., 2017). The CNW films display high transparency, as evidenced by letters to form "CNWs film" underneath such films to be clearly seen in **Figure 1**. In fact, Yamakawa et al. (2017) confirmed that transparent CNW films could be regarded as the green matrix for electrodes.

Morphology of CNW /GN Composites

The cross sectional images of CNW/GN composites after surface fracture were observed under a scanning electron microscope, as depicted in **Figure 2**. Such composite films are densely packed in the film thickness direction, and there are no obvious gaps detected on fracture surfaces despite no applied pressure in the preparation process of films. Apparently, all composite films

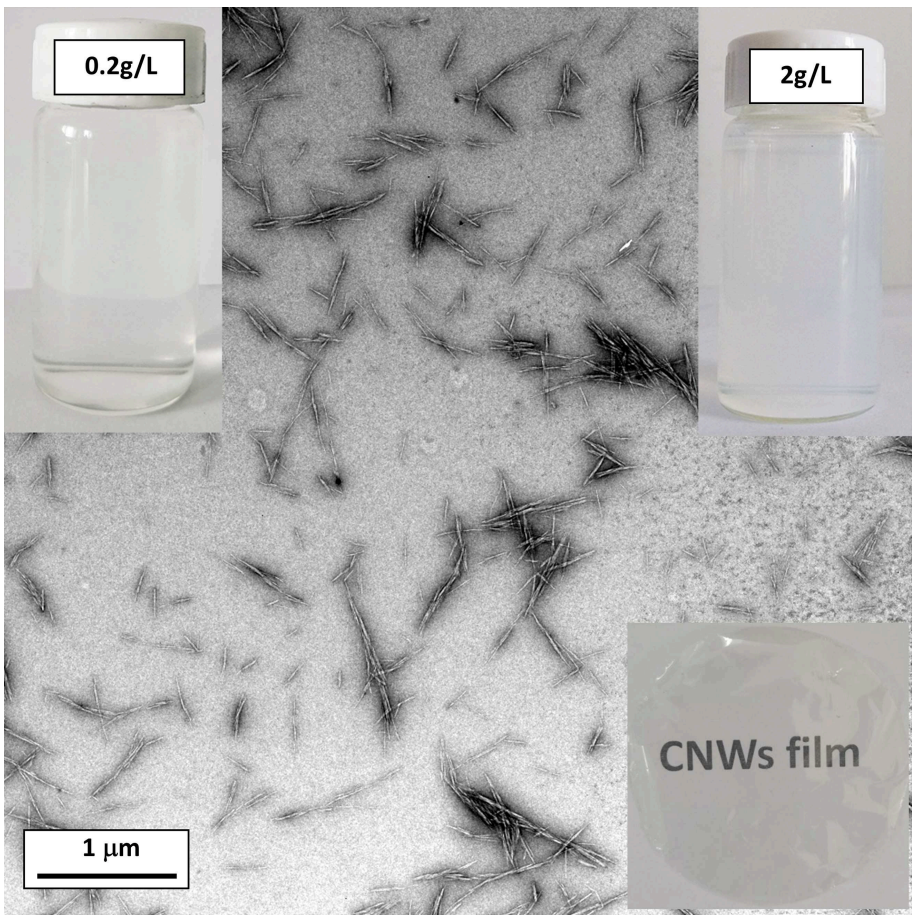

FIGURE 1 | TEM images of dispersed CNWs at the concentration of 0.2 g/L (inset: aqueous CNW suspensions at the CNW concentrations of 0.2 and 2 g/L on the top left and right, respectively, and transparent film on the bottom right).

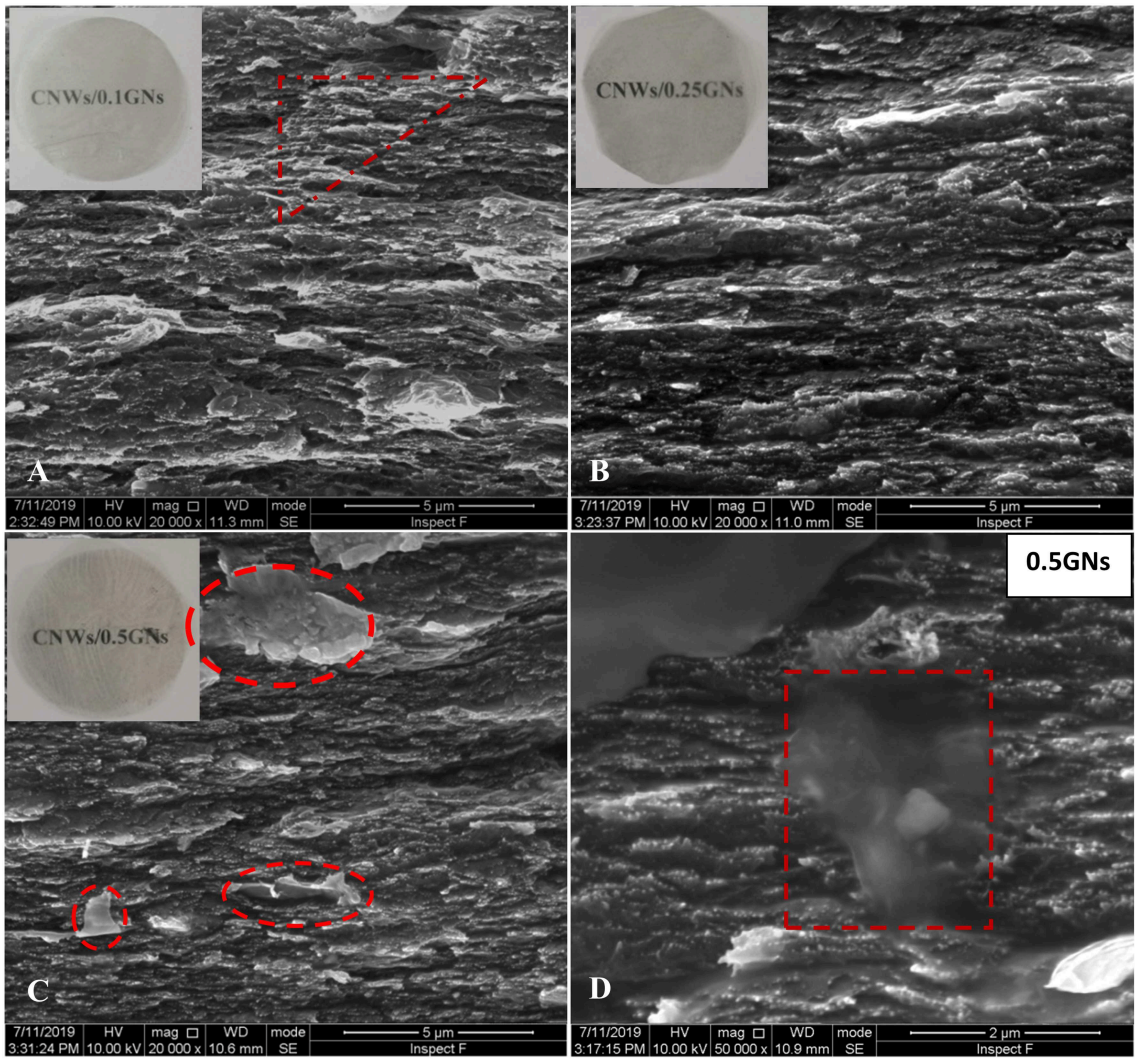

FIGURE 2 | Cross sectional SEM images of CNW/GN composite films at different GN contents: **(A)** 0.1 wt%, **(B)** 0.25 wt%, **(C)** 0.5 wt%, and **(D)** 0.5 wt% (indicating the thin GN sheets attached onto cross sectional surfaces).

appear to mainly comprise randomly oriented CNWs that are closely packed together due to the hydrogen bonding to generate typical layered structures. Many bright dots on SEM images are visible, and can be considered as the tips of individual CNWs. Meanwhile, some shell sheet-like structures become quite evident, indicating good bonding taking place among CNWs alone.

It is not easy to identify GNs particularly in CNW/GN composites at the GN contents of 0.1 and 0.25 wt% shown in **Figures 2A,B**, respectively, which may be ascribed to very uniform GN dispersion in CNW matrices with good interfacial adhesion. When the GN content increases up to 0.5 wt%, GN aggregates in CNW/GN composites appear to be more visible, as marked by red dash frames in **Figures 2C,D**. The lateral size of dispersed GNs is estimated to be 2–5 µm, which is relatively small when compared to that of as-received GN powders, possibly arising from the disintegration effect during the ultrasonication treatment in material preparation. It is worth noting that thin graphene sheets that are marked with read dashed triangular and rectangular frames in **Figure 2D** may fall off on the cross sectional surfaces of composites during the surface fracture process.

The transparent feature of neat CNW films shown in **Figure 1** can be associated with smaller sizes of nanowhiskers than visible wavelength. With increasing the GN content, the color of composite films becomes much darker as expected despite still having good transparency even for composite films reinforced with 0.5 wt% GNs. The transparency of GNs depends primarily on their layered structures. According to Zhu et al. (2014), monolayer graphene grown by chemical vapor deposition (CVD) can achieve very high light transmittance of 97.4% at the normal incidence when the light wavelength of 550 nm

is used. Furthermore, the more number of layers, the lower transmittance is obtained (Zhu et al., 2014). This work clearly proves that the addition of small amounts of GNs can improve the material properties of CNWs without undermining their film transparency.

Thermal Properties

CNWs are well known as a semi-crystalline polymer with a degree of crystallinity in range of 54–88% (Moon et al., 2011). DSC curves in relation to CNW films and CNW/GN composite films are demonstrated in **Figure 3A**. The melting region of CNWs is quite narrow and sharp, which infers their perfect crystalline structures and a narrow range of molecular weight. The T_m of CNWs has been determined to be 209.6°C, which appears to be much lower than that of microcrystalline cellulose (MCC) at 358°C elsewhere (Trache et al., 2014). Such a far lower melting point of CNWs is attributed to their small size and the reduction in molecular weight resulting from the hydrolysis process. As illustrated in **Figure 3A**, when increasing the GN content from 0.1 to 0.25 wt%, the T_m values of composite films are enhanced from 232.8 to 238.9°C despite a slight decline to 235.9°C at the further increasing GN content of 0.5 wt%, which is still higher than that of neat CNW films at 209.6°C. The significant increase in T_m by more than 20°C has been rarely reported in other polymer/graphene composites with only a minor increase in T_m (O'Neil et al., 2014). Such a greatly enhanced T_m level may benefit directly from strong interaction between CNWs and well dispersed rigid GNs that can restrict the molecular chain mobility of CNWs.

In addition to the remarkable increase in T_m, typical degradation temperature of CNWs can also be enhanced with the addition of GNs when characterized by the thermal stability generally applied to assorted polymers in practical applications. Extracted CNWs using sulfuric acid generally exhibit low initial decomposition temperature (T_{id}) when incorporated with sulfate groups (Roman and Winter, 2004). As seen in **Figures 3B,C**, CNWs possesses the T_{id} of only 148.3°C, which is much lower than that of mechanically disintegrated cellulose nanofibers in range of 270–295°C (Okahisa et al., 2018). In comparison, with increasing the GN contents from 0.1, 0.25 to 0.5 wt%, the T_{id} values of CNW/GN composites are increased substantially by 66.4, 78.6, and 87.4°C, respectively. This phenomenon results from the typical retardant effect of GNs on the cleavage of glycosidic linkages of cellulose. It also confirms the existing strong interactions between CNWs and GNs, which has not yet

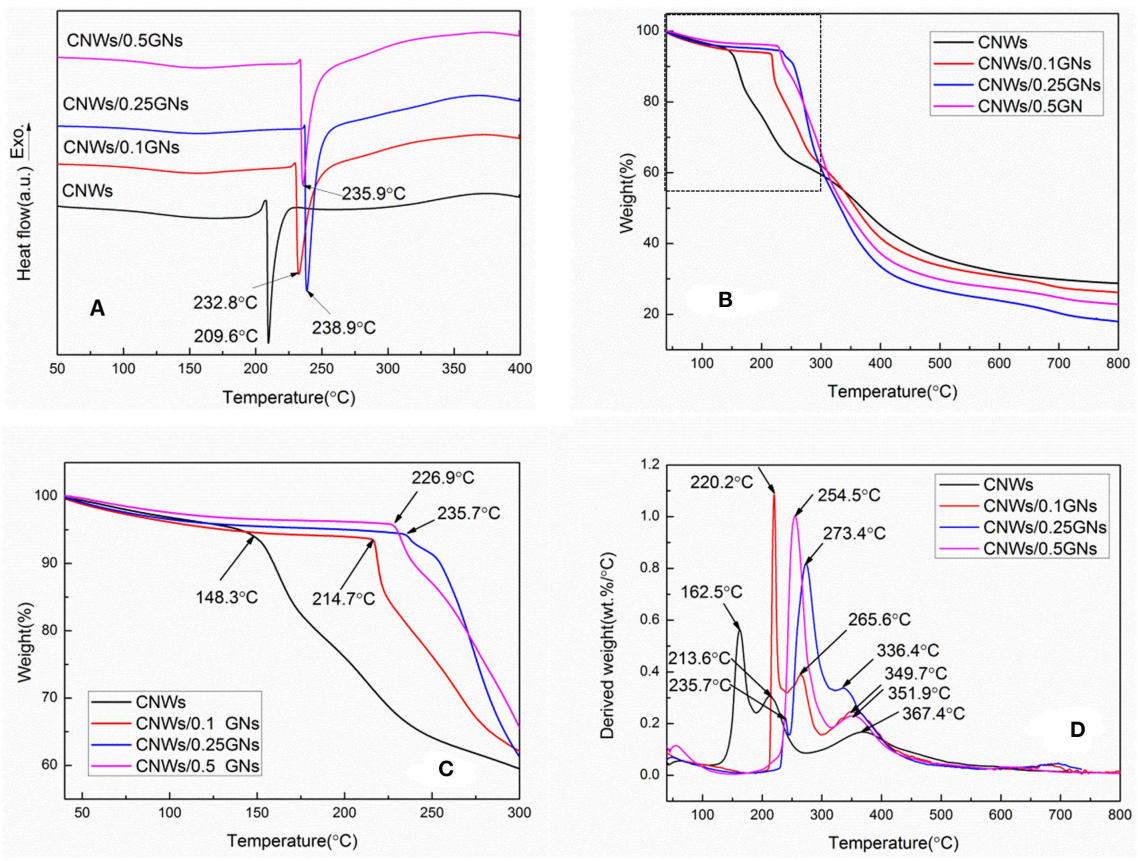

FIGURE 3 | Thermograms of CNW films and CNW/GN composite films: **(A)** DSC curves, **(B)** TGA curves, **(C)** enlarged TGA curve portion within the dash-line block in **(B)**, and **(D)** DTG curves.

been identified in other polymer/graphene composites. More surprisingly, the residual weight of CNWs exceeds those of all CNW/GN composites at 800°C, which can be ascribed to a large number of free end chains during the acid-hydrolysis process (Sofla et al., 2016). Such end chains have been proven to decompose at a lower temperature (Staggs, 2006) leading to an increase in the char yield of CNCs (Piskorz et al., 1989). Moreover, sulfate groups on CNW surfaces in the acid-hydrolysis process may work as flame retardants (Roman and Winter, 2004). Furthermore, Shimizu et al. (2019) also reported the thermal decomposition temperature of 2,2,6,6-tetramethylpiperidine-1-oxyl radical (TEMPO)-mediated oxidized cellulose nanofiber films decreased from 220°C to 182–202°C with increasing the alkyl chain length of quaternary alkyl ammonium (QAs).

Maximum weight loss rate W_{rmax} as a function of temperature can be determined in differential thermogravimetry (DTG) curves of CNW/GN composite films, (**Figure 3D**). There are three typical characteristic DTG peaks detected in composite films. Apparently, the temperature for maximum weight loss rate T_r shifts to higher temperature levels from 162.5 to 273.4°C when increasing the GN contents from 0 to 0.5 wt%. The other two T_r of composite films can be positioned in temperature ranges of 220–270°C and 330–370°C, which presents a similar temperature-increasing tendency with increasing the GN content. Nonetheless, W_{rmax} values of composite films are in range of 0.8–1.0%/°C, which exceed that of neat CNW films at 0.56%/°C, thus leading to lower weight residues at the finish temperature of 800°C.

The relatively low W_{rmax} identified in neat CNW films is associated with their higher char yield in this case (Piskorz et al., 1989). Such results have good agreement with the TGA measurements accordingly. Overall, typical thermal parameters determined in this study are listed in **Table 2**. The existence of sulfate on side chains seems to greatly affect thermal behaviors of CNWs, as evidenced by Ma et al. (2017) suggesting that CNWs under sulfation treatment had T_m and T_{id} values increased by more than 46 and 48°C, respectively.

There is a significant increase in thermal parameters of CNW/GN composites at very low GN contents of 0.1, 0.25, and 0.5 wt%, arising from strong interactions between GN fillers and CNW matrices, which is supported by other studies on 2D materials such as boron nitride (BN) and graphene nanosheets (Li Y. et al., 2015). Under the SEM observation displayed in **Figure 4**, one can clearly see the absorption of CNWs on GN sheets in CNW/GN composites at the GN content of 0.5 wt%. Since cellulose is an amphiphilic polymer, the presence of polar group –OH enables to induce the hydrophilicity while the exposure of –CH moieties gives rise to its hydrophobicity instead. As such, CNWs may interact closely with GNs with dual hydrophobic-hydrophobic effect (Li F. et al., 2015). It has also been suggested that the bonding between CNTs and carboxymethyl cellulose could be due to the π-π interactions (Son and Park, 2018).

TABLE 2 | Thermal parameters, tensile strain at break (ε), tensile strength (σ_t), and electrical conductivity (σ) of CNW films and CNW/GN composite films.

GN (wt%)	T_m (°C)	T_{id} (°C)	ε (%)	σ_t (MPa)	σ (S/m)
0	209.6	143.3	1.4	96.8	–
0.1	232.8	213.5	1.1	105.1	2.5×10^{-8}
0.25	238.9	231.7	1.0	129.4	1.7×10^{-7}
0.5	235.9	231.1	0.8	98.2	4.0×10^{-5}

Electrical Conductivity and Tensile Properties

Transparent and flexible CNW films show low thermal expansion coefficient, which makes them potentially used as packaging films or as substrates for flexible electronics (Yamakawa et al., 2017). The addition of GNs into CNW films increases the electrical conductivity and tensile strength, as shown in **Figure 5**. Neat CNW films as insulating materials undergoes measurement difficulty in electrical conductivity using our equipment, thus its value has not been reported in this study. The electrical conductivity of TEMPO-oxidized cellulose nanofibril (TOCN) reported by Zhan et al. (2019) was 4.8×10^{-12} S/m, indicating typical insulating nature of cellulose films. However, electrical conductivity has been found to increase in range from 2.5×10^{-8} to 4.0×10^{-5} S/m with increasing the GN content from 0.1 to 0.5 wt% shown in **Figure 5A**, which is satisfied with the requirement of anti-static property (Steinert and Dean, 2009). Anti-static property is generally characterized by conductive material surfaces to reduce the static charge induced by internal insulating structures of materials. Our results are close to that of bacterial cellulose (BC)/reduced graphene oxide (RGO) composites at the electrical conductivity level of approximately 1.1×10^{-4} S/m when the RGO content reaches 1.0 wt%, which is two-order higher than that of cellulose nanofiber/1.0 wt% MWCNT composite membranes at 10^{-6} S/m (Feng et al., 2012; Zhang et al., 2019). Luong et al. (2011) reported an even higher conductivity value of 4.8×10^{-4} S/m for amine-modified nanofibrillated cellulose/0.3 wt% RGO nanocomposite papers. All these results reveal the effective improvement in electrical conductivities of cellulose nanocomposites.

Tensile strengths of composite films are enhanced up to 105.1 and 129.4 MPa at the low GN contents of 0.1 and 0.25 wt%, respectively when compared with 96.8 MPa for neat CNW films, as depicted in **Figure 5B**. Conversely, tensile strength of composites declines to 98.2 MPa when incorporated with 0.5 wt% GNs as a result of the inhomogeneity of GN dispersion and typical GN aggregation at relatively high filler content levels. The tensile strain at break for CNW films was determined to be very low at 1.4%. With increasing the GN content up to 0.5 wt%, the corresponding strains for their composites could be reduced modestly to 0.8% in a monotonic manner due to their more brittle nature with the inclusion of GNs as rigid fillers. The relevant data with respect to tensile strength, tensile strain at break and electrical conductivity of composite films are also summarized in **Table 2**. The reinforcing effect of GO and RGO can be more manifested owing to their abundant functional groups (Phiri et al., 2018). Very high tensile strength

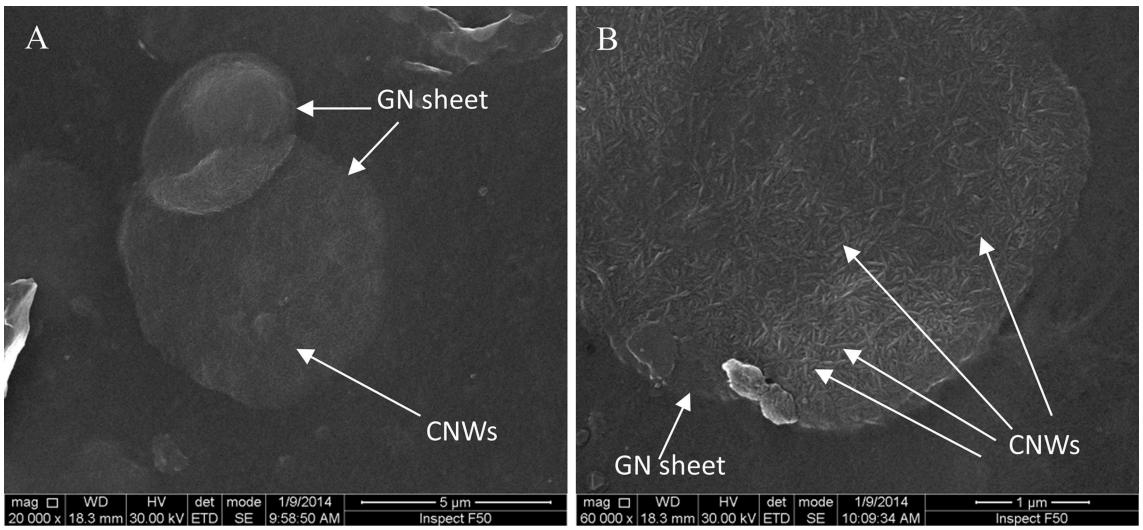

FIGURE 4 | SEM images of CNW adsorption on GN sheets in CNW/GN composite films at the GN content of 0.5 wt%: **(A)** at low magnification of 20,000× and **(B)** at high magnification of 60,000×.

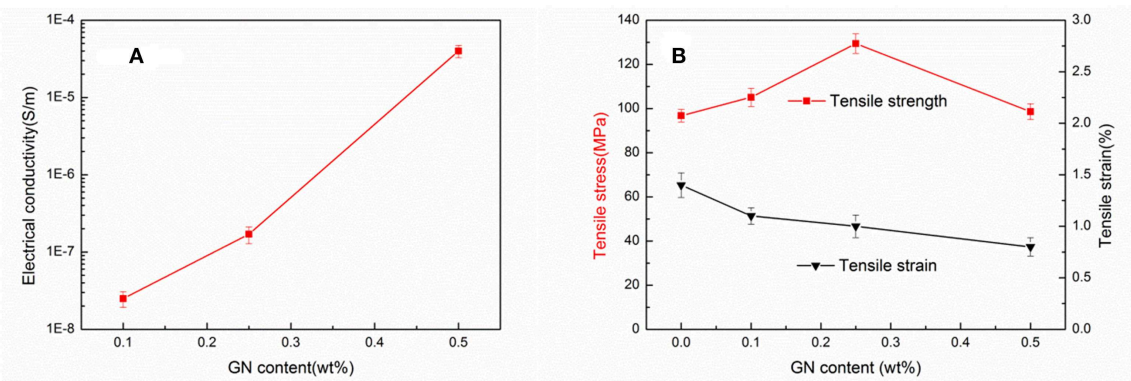

FIGURE 5 | Effect of GN content on **(A)** electrical conductivity and **(B)** tensile strength and tensile strain at break of CNW/GN composite films.

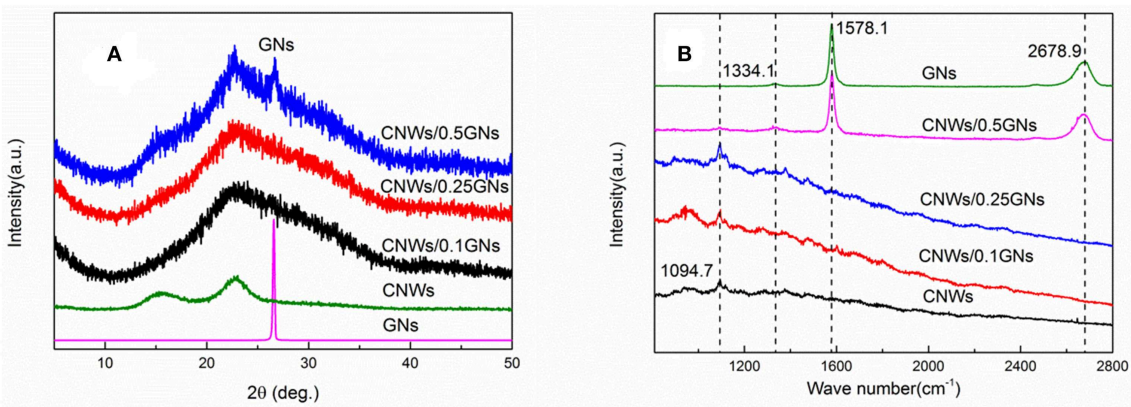

FIGURE 6 | Structural analysis of CNW films and CNW/GN composite films: **(A)** XRD patterns and **(B)** Raman spectra.

of nanofibrillated cellulose (NFC)/1.25 wt% graphene composites was obtained at 351 MPa by means of *in-situ* exfoliation of graphite into graphene sheets in the NFC solutions via the filtration methods (Malho et al., 2012).

Structural Analysis

The crystalline structures of CNW films and CNW/GN composite films are characterized by XRD and Raman spectroscopy, as illustrated in **Figure 6**. High crystalline characteristic of CNWs is evident since their amorphous components are broken down by concentration acid during the hydrolysis process. The characteristic diffraction peaks of composite films positioned at approximately 22.6° corresponding to the reflection of crystal plane (200), are quite broad due to smaller crystalline sizes of CNWs. There is no obvious diffraction of graphene seen in **Figure 6A** in CNW/GN composite films at GN contents of 0.1 and 0.25 wt%, which is believed to be associated with a small amount of uniformly dispersed GNs embedded in CNW matrices (Son and Park, 2018). A tiny peak positioned at 26.8° can be observed on the XRD pattern of CNW/GN composites at the GN content of 0.5 wt%, corresponding to an interlayer distance of 0.34 nm in relation to crystal plane (002). This shows a clear sign of GN aggregation in CNW matrices in good accordance with morphological structures observed earlier. With respect to Raman spectra, the characteristic peak of cellulose is located at 1,095 cm^{-1}, which is consistent with Bulota et al. (2012). The characteristic peaks of GNs can be easily detected in Raman spectra with mainly three bands, namely G band at 1,578 cm^{-1}, D band at 1,334 cm^{-1} and 2D band at 2,679 cm^{-1}, as shown in **Figure 6B**. The vibration of sp^2 carbon atoms yields the appearance of G band as the primary characteristic band of graphene. The disordered vibrational peak of graphene is generally considered as the existence of D band, which is used for characterizing structural defects in graphene samples with rather low intensity in the spectra of GNs. It is clearly indicated that GNs are less defective in this study. Similar to the XRD results, typical GN peak is also not visible until the GN content reaches 0.5 wt% again due to the inclusion of very small amounts of GNs between 0.1 and 0.25 wt%.

CONCLUSIONS

CNW/GN composite films at the small GN contents of 0.1, 0.25, and 0.5 wt% were successfully prepared using solution casting, resulting in their high transparency, enhanced thermal, electrical and mechanical properties. Uniform GN dispersion in CNW matrices in composite films has been found at lower GN contents of 0.1 and 0.25 wt% as opposed to typical GN aggregation at the higher content level of 0.5 wt% along with the resulting decreased tensile strength of composites. The former case leads to the enhancement of tensile strengths of composite films from 96.8 to 129.4 MPa when increasing the GN content from 0 to 0.25 wt% owing to uniform GN dispersion mentioned earlier. GNs as rigid fillers can strongly restrict the molecular chain mobility of CNWs, thus improving the thermal properties of CNW/GN composite films, as evidenced by significantly enhanced T_m and T_{id}. More remarkably, electrical conductivities of composite films are increased by three orders with increasing the GN content from 0.1 to 0.5 wt%. In particular, at the GN content of 0.5 wt%, their electrical conductivity reaches 4.0×10^{-5} S/m with unique anti-static property. Such CNW/GN composite films with good transparency, high mechanical strength and flexibility, excellent thermal and electrical properties can be promising multifunctional materials when particularly targeting electronic applications.

DATA AVAILABILITY STATEMENT

All datasets generated for this study are included in the manuscript/supplementary files.

AUTHOR CONTRIBUTIONS

DL designed the experiments and prepared the manuscript. YL prepared the material samples and conducted XRD and Raman analyses. NM performed thermal analyses (i.e., DSC and TGA) and mechanical tests. DL did structural analysis and electrical conductivity measurements. YD and GS contributed to result discussion and manuscript revision.

REFERENCES

Agate, S., Joyce, M., Lucia, L., and Pal, L. (2018). Cellulose and nanocellulose-based flexible-hybrid printed electronics and conductive composites – a review. *Carbohydr. Polym.* 198, 249–260. doi: 10.1016/j.carbpol.2018.06.045

Bulota, M., Kreitsmann, K., Hughes, M., and Paltakari, J. (2012). Acetylated microfibrillated cellulose as a toughening agent in poly(lactic acid). *J. Appl. Polym. Sci.* 126, E449–E458. doi: 10.1002/app.36787

Carpenter, A. W., de Lannoy, C. F., and Wiesner, M. R. (2015). Cellulose nanomaterials in water treatment technologies. *Environ. Sci. Technol.* 49, 5277–5287. doi: 10.1021/es506351r

Dichiara, A. B., Song, A., Goodman, S. M., He, D., and Bai, J. (2017). Smart papers comprising carbon nanotubes and cellulose microfibers for multifunctional sensing applications. *J. Mater. Chem. A* 5, 20161–20169. doi: 10.1039/C7TA04329E

Drogat, N., Granet, R., Sol, V., Memmi, A., Saad, N., Koerkamp, C. K., et al. (2011). Antimicrobial silver nanoparticles generated on cellulose nanocrystals. *J. Nanopart. Res.* 13, 1557–1562. doi: 10.1007/s11051-010-9995-1

Du, X., Zhang, Z., Liu, W., and Deng, Y. (2017). Nanocellulose-based conductive materials and their emerging applications in energy devices - a review. *Nano Energy* 35, 299–320. doi: 10.1016/j.nanoen.2017.04.001

Esmaeili, C., Abdi, M. M., Mathew, A. P., Jonoobi, M., Oksman, K., and Rezayi, M. (2015). Synergy effect of nanocrystalline cellulose for the biosensing detection of glucose. *Sensors* 15, 24681–24697. doi: 10.3390/s151024681

Feng, Y., Zhang, X., Shen, Y., Yoshino, K., and Feng, W. (2012). A mechanically strong, flexible and conductive film based on bacterial cellulose/graphene nanocomposite. *Carbohydr. Polym.* 87, 644–649. doi: 10.1016/j.carbpol.2011.08.039

Gnanaseelan, M., Chen, Y., Luo, J., Krause, B., Pionteck, J., Pötschke, P., et al. (2018). Cellulose-carbon nanotube composite aerogels as novel thermoelectric materials. *Compos. Sci. Technol.* 163, 133–140. doi: 10.1016/j.compscitech.2018.04.026

He, J., Li, N., Bian, K., and Piao, G. (2019). Optically active polyaniline film based on cellulose nanocrystals. *Carbohydr. Polym.* 208, 398–403. doi: 10.1016/j.carbpol.2018.12.091

Jackson, J. K., Letchford, K., Wasserman, B. Z., Ye, L., Hamad, W. Y, and Burt, H. M. (2011). The use of nanocrystalline cellulose for the binding and controlled release of drugs. *Int. J. Nanomed.* 6, 321–330. doi: 10.2147/IJN.S16749

Jiang, Y., Song, Y., Miao, M., Cao, S., Xin, F. X., Fang, J. H., et al. (2015). Transparent nanocellulose hybrid films functionalized with ZnO nanostructures for UV-blocking. *J. Mater. Chem. C* 3, 6717–6724. doi: 10.1039/C5TC00812C

Jose, J., Thomas, V., Vinod, V., Abraham, R., and Abraham, S. (2019). Nanocellulose based functional materials for supercapacitor applications. *J. Sci. Adv. Mater. Dev*. doi: 10.1016/j.jsamd.2019.06.003. [Epub ahead of print].

Karim, Z., Claudpierre, S., Grahn, M., Oksman, K., and Mathew, A. P. (2016). Nanocellulose based functional membranes for water cleaning: tailoring of mechanical properties, porosity and metal ion capture. *J. Membr. Sci.* 514,418–428. doi: 10.1016/j.memsci.2016.05.018

Ko, J. O., Kima, S. K., Lim, Y. R., Han, J. K., Yoon, Y., Ji, S., et al. (2019). Foldable and water-resist electrodes based on carbon nanotubes/methyl cellulose hybrid conducting papers. *Compos. Part B Eng.* 160, 512–518. doi: 10.1016/j.compositesb.2018.12.060

Latonen, R. M., Määttänen, A., Ihalainen, P., Xu, W., Pesonen, M., Nurmie, M., et al. (2017). Conducting ink based on cellulose nanocrystals and polyaniline for flexographical printing. *J. Mater. Chem. C* 5, 12172–12181. doi: 10.1039/C7TC03729E

Li, F., Mascheroni, E., and Piergiovanni, L. (2015). The potential of nanocellulose in the packaging field: a review. *Packaging Technol. Sci.* 28, 475–508. doi: 10.1002/pts.2121

Li, S., and Lee, P. S. (2017). Development and applications of transparent conductive nanocellulose paper. *Sci. Technol. Adv. Mater.* 18, 620–633. doi: 10.1080/14686996.2017.1364976

Li, Y., Zhu, H., Shen, F., Wan, J., and Hu, L. (2015). Nanocellulose as green dispersant for two-dimensional energy materials. *Nano Energy* 13, 346–354. doi: 10.1016/j.nanoen.2015.02.015

Liew, S. Y., Walsh, D. A., and Thielemans, W. (2013). High total-electrode and mass-specific capacitance cellulose nanocrystal-polypyrrole nanocomposites for supercapacitors. *RSC Adv*. 3, 9158–9162. doi: 10.1039/c3ra41168k

Liu, D. Y., Yuan, X. W., Bhattacharyya, D., and Easteal, A. J. (2010). Characterisation of solution cast cellulose nanofibre – reinforced poly(lactic acid). *eXPRESS. Polym. Lett*. 4, 26–31. doi: 10.3144/expresspolymlett.2010.5

Luo, H., Xie, J., Xiong, L., Zhu, Y., Yang, Z., and Wan, Y. (2019). Fabrication of flexible, ultra-strong, and highly conductive bacterial cellulose-based paper by engineering dispersion of graphene nanosheets. *Compos. Part B Eng.* 162, 484–490. doi: 10.1016/j.compositesb.2019.01.027

Luong, N. D., Pahimanolis, N., Hippa, U., Korhonen, J. T., Ruokolainen, J., Johansson, L. S., et al. (2011). Graphene/cellulose nanocomposite paper with high electrical and mechanical performances. *J. Mater. Chem*. 21, 13991–13998. doi: 10.1039/c1jm12134k

Ma, Y. L., Liu, D. Y., Zhang, X. T., and Sui, G. X. (2017). De-sulfation of cellulose nanowhiskers and its effects on the dispersion behavior of graphene. *J. Dispersion Sci. Technol*. 38, 1798–1803. doi: 10.1080/01932691.2017.1283512

Mahadeva, S. K., Yun, S., and Kim, J. (2011). Flexible humidity and temperature sensor based on cellulose–polypyrrole nanocomposite. *Sens. Actuat. A Phys.* 165, 194–199. doi: 10.1016/j.sna.2010.10.018

Malho, J. M., Laaksonen, P., Walther, A., Ikkala, O., and Linder, M. B. (2012). Facile method for stiff, tough, and strong nanocomposites by direct exfoliation of multilayered graphene into native nanocellulose matrix. *Biomacromolecules* 13, 1093–1099. doi: 10.1021/bm2018189

Meulendijks, N., Burghoorn, M., van Ee, R., Mourad, M., Mann, D., Keul, H., et al. (2017). Electrically conductive coatings consisting of Ag-decorated cellulose nanocrystals. *Cellulose* 24, 2191–2204. doi: 10.1007/s10570-017-1240-y

Moon, R. J., Martini, A., and Simonsen, J., Youngblood J. (2011). Cellulose nanomaterials review: structure, properties and nanocomposites. *Chem. Soc. Rev*. 40, 3941–3994. doi: 10.1039/c0cs00108b

Okahisa, Y., Fukukawa, Y., Ishimoto, K., Narita, C., Intharapichai, K., and Ohara, H. (2018). Comparison of cellulose nanofiber properties produced from different parts of the oil palm tree. *Carbohydr. Polym*. 198, 313–319. doi: 10.1016/j.carbpol.2018.06.089

O'Neil, A., Bakirtzis, D., and Dixon, D. (2014). Polyamide 6/graphene composites: the effect of *in situ* polymerisation on the structure and properties of graphene oxide and reduced graphene oxide. *Eur. Polym. J.* 59, 353–362. doi: 10.1016/j.eurpolymj.2014.07.038

Pang, Z., Sun, X., Wu, X., Nie, Y., Liu, Z., and Yue, L. (2015). Fabrication and application of carbon nanotubes/cellulose composite paper. *Vacuum* 122, 135–142. doi: 10.1016/j.vacuum.2015.09.020

Phiri, J., Johansson, L. S., Gane, P., and Malone, T. (2018). A comparative study of mechanical, thermal and electrical properties of graphene-, graphene oxide- and reduced graphene oxide-doped microfibrillated cellulose nanocomposites. *Compos. Part B Eng.* 147, 104–113. doi: 10.1016/j.compositesb.2018.04.018

Piskorz, J., Radlein, D. S. A., Scott, D. S., and Czernik, S. (1989). Pretreatment of wood and cellulose for production of sugars by fast pyrolysis. *J. Anal. Appl. Pyrol.* 16, 127–142. doi: 10.1016/0165-2370(89)85012-0

Roman, M., and Winter, W. T. (2004). Effect of sulfate groups from sulfuric acid hydrolysis on the thermal degradation behavior of bacterial cellulose. *Biomacromolecules* 5, 1671–1677. doi: 10.1021/bm034519+

Sadasivuni, K. K., Ponnamma, D., Ko, H. U., Kim, H. C., Zhai, L., and Kim, J. (2016). Flexible NO_2 sensors from renewable cellulose nanocrystals/iron oxide composites. *Sens. Actuat. B Chem.* 233, 633–638. doi: 10.1016/j.snb.2016.04.134

Shimizu, M., Kusumi, R., Saito, T., and Isogai, A. (2019). Thermal and electrical properties of nanocellulose films with different interfibrillar structures of alkyl ammonium carboxylates. *Cellulose* 26, 1657–1665. doi: 10.1007/s10570-018-2155-y

Sofla, M. R. K., Brown, R. J., Tsuzuki, T., and Rainey, T J. (2016). A comparison of cellulose nanocrystals and cellulose nanofibres extracted from bagasse using acid and ball milling methods. *Adv. Nat. Sci. Nanosci. Nanotechnol.* 7:035004. doi: 10.1088/2043-6262/7/3/035004

Son, Y. R., and Park, S. J. (2018). Green preparation and characterization of graphene oxide/carbon nanotubes-loaded carboxymethyl cellulose nanocomposites. *Sci. Rep.* 8:17601. doi: 10.1038/s41598-018-35984-2

Staggs, J. E. J. (2006). Discrete bond-weighted random scission of linear polymers. *Polymer* 47, 897–906. doi: 10.1016/j.polymer.2005.11.085

Steinert, B. W., and Dean, D. R. (2009). Magnetic field alignment and electrical properties of solution cast PET–carbon nanotube composite films. *Polymer* 50, 898–904. doi: 10.1016/j.polymer.2008.11.053

Trache, D., Donnt, A., Khimeche, K., Benelmir, R., and Brosee, N. (2014). Physico-chemical properties and thermal stability of microcrystalline cellulose isolated from Alfa fibres. *Carbohydr. Polym*. 104, 223–230. doi: 10.1016/j.carbpol.2014.01.058

Xing, J., Tao, P., Wu, Z., Xing, C., Liao, X., and Nie, S. (2019). Nanocellulose-graphene composites: a promising nanomaterial for flexible supercapacitors. *Carbohydr. Polym*. 207, 447–459. doi: 10.1016/j.carbpol.2018.12.010

Yamakawa, A., Suzuki, S., Oku, T., Enomoto, K., Ikeda, M., Rodrigue, J., et al. (2017). Nanostructure and physical properties of cellulose nanofiber-carbon nanotube composite films. *Carbohydr. Polym*. 171, 129–135. doi: 10.1016/j.carbpol.2017.05.012

Yuan, Z., Zhang, J., Jiang, A., Lv, W., Wang, Y., Geng, H., et al. (2015). Fabrication of cellulose self-assemblies and high-strength ordered cellulose films. *Carbohydr. Polym*. 117, 414–421. doi: 10.1016/j.carbpol.2014.10.003

Zhan, H., Peng, N., Lei, X., Huang, Y., Li, D., Tao, R. (2018). UV-induced self-cleanable TiO_2/nanocellulose membrane for selective separation of oil/water emulsion. *Carbohydr. Polym.* 201, 464–470. doi: 10.1016/j.carbpol.2018.08.093

Zhan, Y., Xiong, C., Yang, J., Shi, Z., and Yang, Q. (2019). Flexible cellulose nanofibril/pristine graphene nanocomposite films with high electrical conductivity. *Compos. Part A Appl. Sci. Manuf.* 119, 119–126. doi: 10.1016/j.compositesa.2019.01.029

Zhang, H., Sun, X., Hubbe, M. A., Pal, L. (2019). Highly conductive carbon nanotubes and flexible cellulose nanofibers composite membranes with semi-interpenetrating networks structure. *Carbohydr. Polym.* 222:115013. doi: 10.1016/j.carbpol.2019.115013

Zhang, X. T., Liu, D. Y., Ma, Y. L., Nie, J., and Sui, G. X. (2017). Super-hydrophobic graphene coated polyurethane (GN@PU) sponge with great oil-water separation performance. *Appl. Surf. Sci.* 422, 116–124. doi: 10.1016/j.apsusc.2017.06.009

Zhang, X. T., Liu, D. Y., and Sui, G. X. (2018). Superamphiphilic polyurethane foams synergized from cellulose ers and graphene nanoplatelets. *Adv. Mater. Interf.* 5:1701094. doi: 10.1002/admi.201701094

Zhu, S. E., Yuan, S., and Janssen, G. C. A. M. (2014). Optical transmittance of multilayer graphene. *Europhys. Lett.* 108:17007. doi: 10.1209/0295-5075/108/17007

Conflict of Interest: The authors declare that the research was conducted in the absence of any commercial or financial relationships that could be construed as a potential conflict of interest.